Research Article | Vol. 2, No. 11 / 15 November 2019 / OSA Continuum 3288

Coupled microstrip-cavities under oblique incidence of semi-guided waves: a lossless integrated optical add-drop filter

LENA EBERS,* MANFRED HAMMER, MANUEL B. BERKEMEIER, ALEXANDER MENZEL, AND JENS FÖRSTNER

Paderborn University, Theoretical Electrical Engineering, Warburger Str. 100, 33098 Paderborn, Germany
**lena.ebers@uni-paderborn.de*

Abstract: We investigate optical microresonators consisting of either one or two coupled rectangular strips between upper and lower slab waveguides. The cavities are evanescently excited under oblique angles by thin-film guided, in-plane unguided waves supported by one of the slab waveguides. Beyond a specific incidence angle, losses are fully suppressed. The interaction between the guided mode of the cavity-strip and the incoming slab modes leads to resonant behavior for specific incidence angles and gaps. For a single cavity, at resonance, the input power is equally split among each of the four output ports, while for two cavities an add-drop filter can be realized that, at resonance, routes the incoming power completely to the forward drop waveguide via the cavity. For both applications, the strength of the interaction is controlled by the gaps between cavities and waveguides.

1. Introduction

Optical microresonators are used for many functionalities in integrated optics, e.g. for wavelength modulation, switching, or filtering purposes. Due to their compact size, wide spectral tunability and strong light confinement they gained huge interest. They are one of the main building blocks in silicon photonics integrated circuits, mainly in the area of optical telecommunication (see [1] and references cited therein). One of the basic configurations is a four-port system consisting of two parallel straight waveguides, serving as input and output buses, evanescently coupled to a cavity placed in between. Most of the earlier concepts deal with circular cavities [2–7], but structures with rectangular shapes have gained interest as well [8–13].

The disadvantage of these concepts, already when considered as 2-D models, is that the devices are inherently lossy [1]. Furthermore, specific dimensions are required to obtain the desired resonant behavior of sufficient quality [8–10]. In this work we reconsider these devices in a 2.5-D setting, meaning excitation by an incoming wave under an oblique angle θ as illustrated in Figure 1(a). We will show that as a result, losses are suppressed at sufficiently high angles θ and rather arbitrary cavity parameters can be selected.

We consider microresonators consisting of a rectangular, standing wave micro-strip cavity of fixed dimensions $w \times h$, which is surrounded by two slab waveguides of identical thickness d, at the same but variable distance g to the cavity as shown in Figure 1(b). In contrast to standard notions of open dielectric cavities with a more or less confined resonance mode, in the present 2.5-D setting the strip is infinitely extended along its axis and supports a mode that is propagating in z-direction. The resonances observed in our structures are based on these lossless guided modes. The structure is excited by the fundamental TE mode of the lower waveguide, while the upper slab acts as the receiver. The incident wave reaches the cavity strip under an incidence angle θ with respect to the x-axis in the x-z-plane. We consider "semi-guided", vertically (y) guided, laterally (x, z) unguided waves. The theory [11,14–20] behind the "oblique incidence of

#373687 https://doi.org/10.1364/OSAC.2.003288
Journal © 2019 Received 25 Jul 2019; revised 27 Sep 2019; accepted 2 Oct 2019; published 11 Nov 2019

OSA CONTINUUM

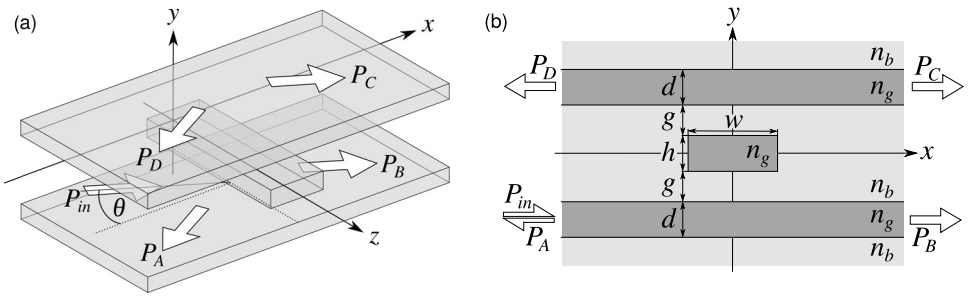

Fig. 1. Oblique evanescent excitation of a dielectric resonator with rectangular micro-strip cavity; schematic view (a) and cross section view (b). The incoming semi-guided wave propagates under an incidence angle θ normal to the cavity. Outgoing optical waves are either directly transmitted, forward or backward dropped, or reflected. $P_\mathrm{A}, P_\mathrm{B}, P_\mathrm{C}$ and P_D indicate the outgoing power at the respective ports. Material parameters correspond to a SOI design with refractive indices $n_\mathrm{g} = 3.45$ in the guiding layers and $n_\mathrm{b} = 1.45$ in the claddings and the gaps between the layers. Waveguide thicknesses are defined as $d = h = 0.22\,\mu$m with a cavity width of $w = 0.5\,\mu$m and variable gap distance g. Incoming wave is the TE mode for vacuum wavelength $\lambda = 1.55\,\mu$m.

semi-guided waves" is reviewed in Section 2. All necessary parameters are listed in the caption of Figure 1 for a typical SOI waveguide design.

While a single resonator cavity only drops a quarter of the input power in each output port, a configuration with two cavities can be configured to transfer all incoming signal power to a single receiver port, i.e. can realize an optical add-drop filter [21]. Hence, after discussing a single cavity in Section 3, we will expand the configuration by a second cavity in Section 4. We are going to analyze the structures for different geometry parameters.

This work takes up our earlier results from [11], where we considered a simpler structure without the upper slab waveguide (two-port system) and only the single cavity case. Such a structure works as a system with a non-radiating bound state (the guided mode of the rectangular cavity) and a wave continuum (guided by the slab). Hence, this realizes what we called "bound state coupled to a continuum" in [11]. We adopt the waveguide parameters, especially we fix the size of the cavity, for our present studies.

2. Oblique excitation of a microresonator

For a standard 2-D setting, meaning $\theta = 0°$, the configuration results in a scalar problem for either TE or TM polarized waves. For the more general approach of oblique incidence $\theta \neq 0°$, the polarizations become coupled which results in a vectorial 2.5-D problem. For that case, we can define critical angles beyond which scattering to non guided modes or/and TM excitation is fully suppressed. Here, we will shortly discuss the theory behind these critical angles. For a more detailed analysis we refer to Refs. [11,14–20].

We basically assume fields of time dependence $\sim \exp(\mathrm{i}\omega t)$ with angular frequency ω given by the vacuum wavelength $\lambda = 2\pi/k = 2\pi\mathrm{c}/\omega$, for vacuum wavenumber k and speed of light c. For the considered waveguide thickness ($d = 0.22\,\mu$m) both slab waveguides guide the fundamental TE and TM modes with effective mode indices $N_\mathrm{TE} = 2.823$ and $N_\mathrm{TM} = 1.725$. The incoming semi-guided TE wave has a field dependence $\sim \mathbf{\Psi}_\mathrm{in}(k_z, y)\ \exp(-\mathrm{i}(k_x x + k_z z))$, where the wavenumbers are determined by the incidence angle θ. According to Figure 1(a) the wavenumber in lateral direction is defined by $k_z = kN_\mathrm{TE}\sin\theta$ and in propagation direction by $k_x = kN_\mathrm{TE}\cos\theta$ with the condition $k^2N_\mathrm{TE}^2 = k_x^2 + k_z^2$.

OSA CONTINUUM

The whole waveguide structure is homogeneous/constant in z-direction, such that, at all positions, the overall field solution can be restricted to a single Fourier component given by the in-plane wavenumber k_z. Hence, the outgoing fields share this dependence and can be written in a similar form as the incoming field by $\sim \mathbf{\Psi}_{\mathrm{out}}(k_z, .)\ \exp(-\mathrm{i}(k_\xi \xi + k_z z))$. Here, ξ describes an arbitrary outgoing propagation direction. This formalism is valid for all propagating waves as well as all non-guided, radiated waves.

The condition $k^2 N_{\mathrm{out}}^2 = k_\xi^2 + k_z^2 = k_\xi^2 + k^2 N_{\mathrm{TE}}^2 \sin^2\theta$ still has to hold for each outgoing wave propagating in ξ-z-direction. Depending on the involved outgoing mode and its effective mode index N_{out}, the outgoing mode is either a propagating mode ($k_\xi^2 > 0$) or an evanescent mode ($k_\xi^2 < 0$). By considering the detailed reasonings of [11,14–20] critical angles can be defined by $\sin\theta_{\mathrm{crit}} = N_{\mathrm{out}}/N_{\mathrm{TE}}$, beyond which no power transfer to that specific outgoing mode is given. In that case the mode becomes evanescent and does not carry any optical power away from the discontinuity. For the Si/SiO_2 configuration considered in this work two critical angles are relevant:

- θ_{b}: All radiative, non-guided ("cladding"-) modes have effective mode indices $N_{\mathrm{out}} \leq n_{\mathrm{b}}$. For $\theta \geq \theta_{\mathrm{b}} = 30.9°$ ($\sin\theta_{\mathrm{b}} = n_{\mathrm{b}}/N_{\mathrm{TE}}$) these modes become evanescent and radiation losses are completely suppressed.
- θ_{TM}: The reflected and transmitted fundamental TM mode becomes evanescent for $\theta \geq \theta_{\mathrm{TM}} = 46.3°$ ($\sin\theta_{\mathrm{TM}} = N_{\mathrm{TM}}/N_{\mathrm{TE}}$). The input power is then fully reflected and/or transmitted into one of the four outgoing TE modes.

3. Single cavity resonators

We will start by analyzing the configuration regarding scattering parameters. The finite element solver of COMSOL Multiphysics [22] is used to solve the frequency domain Maxwell's equations. Port boundary conditions are applied to excite and absorb plane waves consisting of a specific mode index – value to be stated – and direction. Furthermore they are also used to easily calculate scattering parameters. To simulate an infinite structure with open boundaries perfectly matched layers (PMLs) are added around the whole structure. By defining an out-of-plane wavenumber k_z COMSOL is able to simulate oblique incidence, hence this represents the former 2.5-D setting.

First, we will start with the mode analysis of the resonator cavity. For the parameters listed in the caption of Figure 1 COMSOL predicts a mode index of the fundamental guided TE mode of $N_{\mathrm{m}} = 2.4192$. A fundamental TM mode is supported as well, but has a lower mode index, i.e. corresponds to a resonance at an angle outside our present range of interest. This wavenumber can be translated to an incidence angle θ_{m} in line with the argumentation of Section 2 by $kN_{\mathrm{m}} = kN_{\mathrm{TE}}\sin\theta_{\mathrm{m}}$, such that the wavenumber k_z of the incoming wave matches the wavenumber of the cavity mode. This results in a value of $\theta_{\mathrm{m}} = 58.99°$. By exciting the input slab at angles around θ_{m} the mode in the cavity is excited and resonant behavior can be observed. Figure 2(a) shows respective sweeps over θ for different gap distances and Figure 2(b) illustrates some corresponding fields at resonance angle θ_{r}.

Under an incidence angle of $\theta = 0°$, at normal incidence, COMSOL predicts a transmitted power of about 99% to port B ($P_{\mathrm{B}} = 98.93\%$). Power transfer to the upper forward and backward port is in the range of 10^{-4} and thus hardly present. Radiation losses appear but remain negligible. Hence for this case the waves just pass by below the cavity without any disturbances.

For increasing incidence angle this behavior is changing according to the curves of Figure 2(a). In all cases the range of incidence angles is above the critical angles $\theta_{\mathrm{b}} = 30.9°$ and $\theta_{\mathrm{TM}} = 46.3°$, thus excitation of TM modes is suppressed and the configuration is lossless. For a fixed gap size there exists a specific incidence angle θ_{r} for which the power transfer to each port is equal, thus the power is quartered ($P_{\mathrm{A}} = P_{\mathrm{B}} = P_{\mathrm{C}} = P_{\mathrm{D}} = 25\%$). This behavior is observed for excitation angles close to θ_{m}. At resonance, the incoming slab mode excites the mode in the strip waveguide, which

OSA CONTINUUM

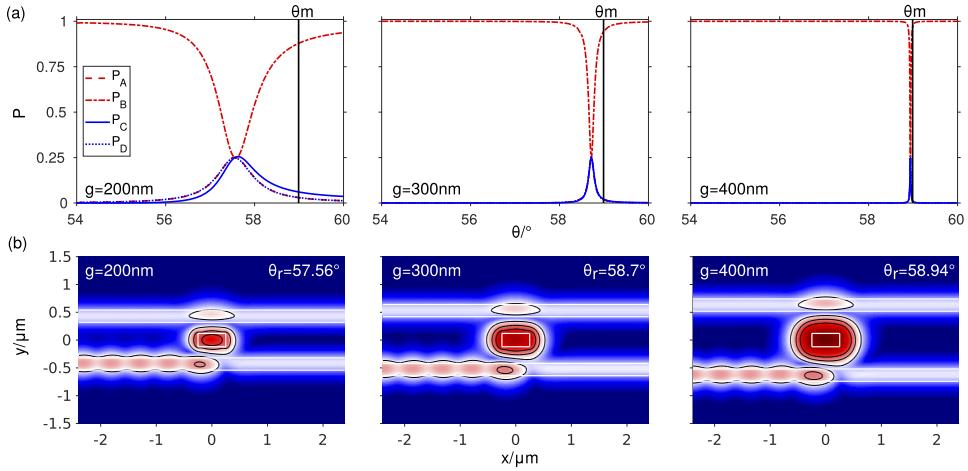

Fig. 2. (a) Relative transmission / reflection power levels of a microresonator with a single cavity for different gaps $g \in \{200, 300, 400\}$ nm as a function of the incidence angle θ; (b) field plots of the absolute electric field $\log_{10}|\boldsymbol{E}|$ at resonant angle θ_r for the corresponding fixed gap distances g from (a). The contour lines indicate the levels of 2%, 5% and 10% of the overall absolute field maximum.

in turn radiates equally into both slab waveguides along the positive and negative x-directions. Since only one cavity mode exists, there is only one component decaying along those directions such that no complete destructive interference and thus no power cancellation at any specific port is possible. Therefore this leads to the same output power at each port [23,24].

The resonance angle θ_r deviates from θ_m especially for small gap distances. This is due to the presence of the slab waveguides and is explained by coupling induced resonance shifts [25]. For larger gap distances the angle θ_r moves closer to θ_m and the resonance sharpens. The curves for P_A, P_C and P_D become more and more similar, thus they overlap in the plots. Some corresponding fields are shown in Figure 2(b) at resonance angle θ_r. As can be observed, the field shape in the cavity resembles more and more the guided TE mode of the cavity. We chose a logarithmic scaling of the absolute electric field value to show the field in the slabs, which is much smaller than the field maximum in the cavity, especially for increasing gap distance.

The resonator characteristics are controlled by the interaction between the cavity and the slabs, hence depend strongly on the gap distance g. Figure 3(a) shows the resonant angles θ_r as a function of the gap g. As expected, the resonance angle converges against the angle of the cavity mode θ_m for increasing gap size. Additionally the field strength in the cavity is considered in

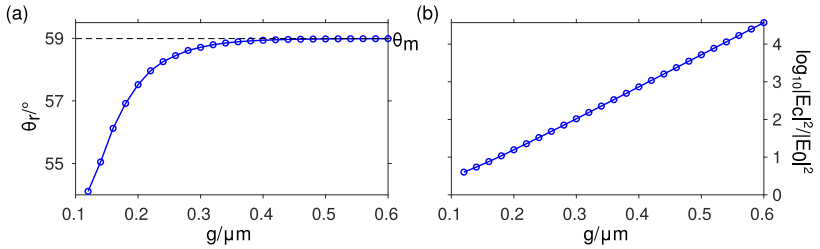

Fig. 3. Resonance angles θ_r with equal outgoing power on each port (a) and absolute square of the electric field maximum $\boldsymbol{E}_c$ in the center of the cavity relative to the absolute field maximum $\boldsymbol{E}_0$ of the isolated slab at $\theta = 58.99°$ (b) versus the gap g.

OSA CONTINUUM

Figure 3(b). Illustrated is the ratio of the electric field magnitude in the center of the cavity at resonance, normalized to the field at the center of the incoming slab without cavity and upper slab. The value grows exponentially for increasing gap distance, hence predicts a high Q-factor of the resonator. This behavior can also be observed in Figure 2(b), for which reason we chose the logarithmic scaling for those plots. For further details and properties of a single rectangular microcavity evanescently excited by oblique semi-guided waves, we refer to our earlier published results in [11].

4. Filter configuration with two identical cavities

A single cavity is not able to transfer all incoming power to one drop port at resonance, and thus is not directly suitable for a configuration as an add-drop filter. Therefore, following the concepts from [10], we will expand the structure to two identical rectangular cavities separated by a horizontal distance s as shown in Figure 4. This configuration is able to route all input power to a single channel [10,23,24,26]. We consider a symmetric structure with identical gap g between the slabs and both cavities. Waveguide parameters are again adopted from Figure 1.

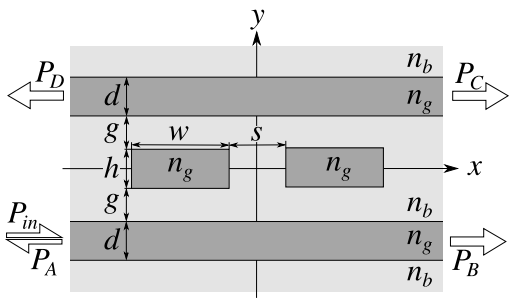

Fig. 4. Cross section view of a symmetric four-port configuration consisting of two identical cavities with dimensions $w \times h$ at distance s. Input and receiver slabs of thickness d are separated by the distance g from the cavities. Specific waveguide parameters are adopted from Figure 1. As before, the incoming semi-guided TE wave propagates at angle θ as demonstrated in Figure 1(a).

We will start by analyzing the resonator cavities regarding their guided modes, which strongly depend on the inter-cavity separation s. For a small distance we have to handle the two strips as a coupled waveguide system that supports one mode ("supermode") with even symmetry, and a second mode with odd symmetry (with respect to the symmetry plane $y = 0$). Their effective refractive indices are given by $N_{\mathrm{m,e}}$ (even) and $N_{\mathrm{m,o}}$ (odd). The values differ from each other, e.g. for a cavity distance of $s = 530\,\mathrm{nm}$ the COMSOL mode solver predicts values of $N_{\mathrm{m,e}} = 2.4199$ ($\theta_{\mathrm{m,e}} = 59.01°$) and $N_{\mathrm{m,o}} = 2.4186$ ($\theta_{\mathrm{m,o}} = 58.95°$). For increasing cavity distance the system is becoming more and more decoupled. Hence, the strips must be treated as two separate systems that do not directly affect each other. Therefore the effective refractive indices of the two decoupled modes are inherently given by the index $N_{\mathrm{m}} = 2.4192$ of the single cavity, or an incidence angle of $\theta_{\mathrm{m}} = 58.99°$. The values $N_{\mathrm{m,e}}$ and $N_{\mathrm{m,o}}$ slowly converge to the value of the single cavity for increasing cavity distance, leading to a decoupled system.

4.1. Directly coupled cavities

First we look at systems with comparably small distance s, where a direct interaction between the cavity strips must be assumed. The dotted line in Figure 5(b) illustrates the outgoing relative power to port C over the incidence angle θ for a quite narrow cavity distance $s = 100\,\mathrm{nm}$. For this sufficiently small distance the cavity modes are coupled and we can thus find an even and

OSA CONTINUUM

odd mode, with corresponding incidence angles $\theta_{m,e}$ and $\theta_{m,o}$, as mentioned before. By exciting the structure at angles close to $\theta_{m,e}$ or $\theta_{m,o}$, resonances can be identified where either the even or the odd mode is excited in the cavities. This results in an identical behavior as for the single cavity from Section 3, leading to a quarter of input power to each output port. As before, the two resonance peaks get sharper and narrower for increasing gap g. Note that for a small gap distance, e.g. $g = 200\,\text{nm}$, the peaks already overlap, so that it is not possible to excite the odd mode without the even mode. Hence, this does not lead to a quarter of the input power in each output port.

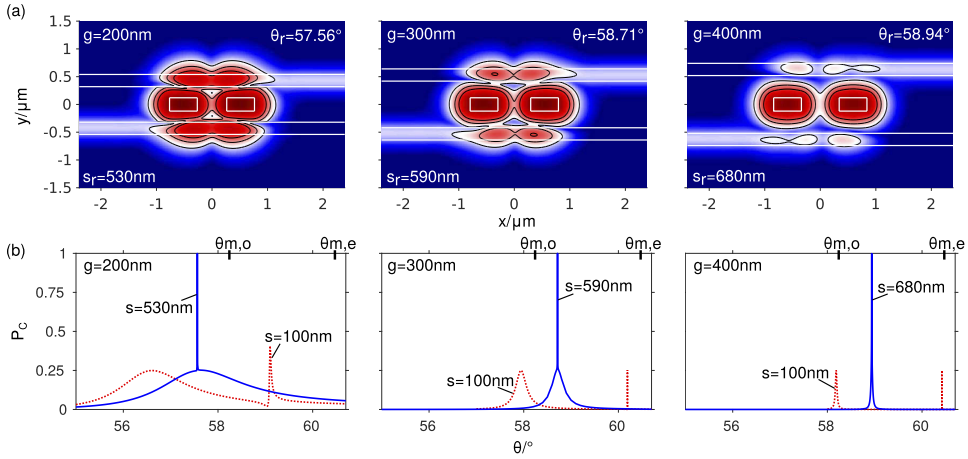

Fig. 5. (a) Field plots of the absolute electric field $\log_{10}|\boldsymbol{E}|$ at resonance (θ_r, s_r) for different gaps $g \in \{200, 300, 400\}$ nm. Contour lines indicate the levels at 2%, 5% and 10% of the overall field maximum. (b) Outgoing power P_C in the forward drop port over the incidence angle θ for different cavity distances s around the resonance (θ_r, s_r) for the corresponding gaps from (a). The angles $\theta_{m,e}$ and $\theta_{m,o}$ associated with the even (e) and odd (o) supermodes of the coupled strips at $s = 100\,\text{nm}$ are indicated.

Next, we adapt the procedure that led to Figure 3(a) to find resonant states (θ_r, s_r) for the configuration with two cavities. To that end, we fix the gap distance g and search for incidence angles θ and cavity distances s that lead to full power drop in the forward port ($P_C = 1$). Figure 5(a) shows plots of the electric field (again in logarithmic scale) at resonance (θ_r, s_r) for gap distances $g \in \{200, 300, 400\}$ nm. Additionally, the solid line in Figure 5(b) illustrates the outgoing power to port C as a function of the incidence angle θ for the cavity distance s_r that leads to resonance. Here, at a distance s_r and angle θ_r, the position of the two peaks of the even and odd mode coincide, and the structure realizes full power drop to the forward port P_C by exciting these modes simultaneously.

Analogously to a single cavity at resonance, here the incoming slab mode excites the even and odd modes in the cavity, which in turn leak into the slab waveguides in both directions. However, now two supermodes are relevant. At resonance, the even mode excites the slab modes in forward and backward directions with the same phase, while exciting the odd mode results in a π-phase-shift between the slab modes in forward direction and those in backward direction. By combining the two processes (because of degeneracy the two independent processes appear simultaneously at resonance) the waves in backward direction get fully canceled due to the phase shift. Furthermore the incoming wave interferes destructively with the forward slab mode excited by the cavities, which results in a full power drop into the upper waveguide [23,24].

OSA CONTINUUM

4.2. Interpretation in terms of leaky modes

Especially in Figure 5(b) for $s = 100$ nm one observes on the one hand a wide hill positioned around the incidence angle that excites the odd mode and on the other hand a narrow peak that corresponds to the even mode at a larger incidence angle. To explain the different shapes of these resonances it is useful to determine the leaky even and odd modes of the overall structure, including now both strip-cavities and slab waveguides. The calculated effective index values N_s are shown in Figure 6 as a function of the separation s. Depicted are the real (a) and imaginary part (b) of the even (solid line) and odd (dashed line) modes.

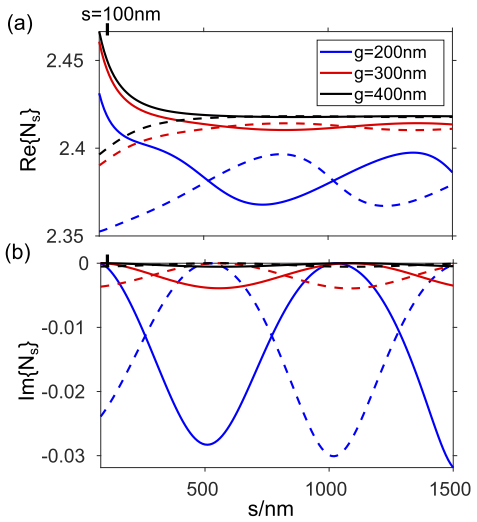

Fig. 6. Real (a) and imaginary (b) part of the effective index N_s for the even (solid line) and odd (dashed line) modes for the overall structure (including cavities and slabs) depending on the separation s for different gaps $g \in \{200, 300, 400\}$ nm.

For the separation of $s = 100$ nm the imaginary part of the effective index of the even mode is approximately zero – nearly a guided mode –, while for the odd mode the absolute value of the imaginary part is comparably large. This relates to the leakage of the modes and predicts the broad resonance for the leaky odd mode. In contrast, the peak for the even mode is very narrow, as it hardly leaks.

The periodic behavior with respect to the separation s of the imaginary part in Figure 6(b) for the even and odd mode can be predicted by analytical arguments. Both cavities radiate into the slab waveguides, where the fields overlap. For specific separations s this interference is either destructive or constructive, depending on whether the even or odd mode is considered. Because of the phase shift of the even and odd modes, the curves are shifted by half a period.

Furthermore, the degeneracy at resonance and its corresponding resonance angle, observed in Section 4.1, Figure 5, of the two modes can be clarified with the mode analysis of the overall structure. The modes are degenerate as the real parts match. According to Figure 6(a) the curves cross approximately at a separation of 520 nm, 585 nm and 680 nm for the given gaps of 200 nm, 300 nm and 400 nm. The effective indices at the intersection points can be converted into angles of 57.53°, 58.72° and 58.94°. These values agree well with the before calculated resonance states (θ_r, s_r) (see Figure 5(a)).

This procedure is also applicable to the single cavity resonator from Section 3. Mode analysis with COMSOL of the composite system with only a single cavity predicts one leaky mode with complex effective index that is different for each gap. Translating the real parts of the wavenumbers again to corresponding angles, one receives values of 57.54°, 58.71° and 58.94°

OSA CONTINUUM

for the given gaps $g \in \{200, 300, 400\}$ nm. These angles also deviate only slightly from the calculated resonance angles θ_r in Figure 2(b). Note, however, that fundamentally different problems – leaky eigenvalue problem and mode propagation problem – are considered.

4.3. Wavelength spectra

Respective sweeps over the wavelength are shown in Figure 7 for the configurations with the (θ_r, s_r)-parameters of Figure 5(a). Full power transfer is achieved at the resonance wavelength $\lambda_r = 1.55\,\mu$m. Thus, for fixed geometrical parameters and fixed angle this represents an add-drop filter for one specific wavelength in the spectral range as considered.

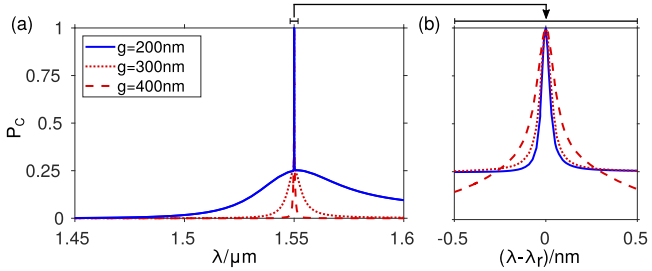

Fig. 7. (a) Outgoing power scans P_C over the wavelength λ for different gap distances g at resonance with the corresponding values (θ_r, s_r) adopted from Figure 5(a). (b) Enlargement of the resonance peak for a smaller range of wavelengths around the resonance wavelength $\lambda_r = 1.55\,\mu$m.

As for the angular spectra in Figure 5(a), we observe resonance features consisting of a wider lower "hill", leveling out at $P_C = 0.25$, with a superimposed narrower peak that reaches $P_C = 1$. For growing gap g, the lower hills become narrower, just as the resonances of the single cavity resonators in Figure 2. Contrarily, the upper peaks appear to widen slightly (cf. Figure 7(b)), when the gap is increased. An analogous behavior (not explicitly shown) is observed for the angular spectra in Figure 5(b). This can be understood, if one attributes the width of the hill primarily to the *width* of the elementary strip resonances, while the width of the peaks is being determined by the *positions* of the resonances associated with the individual cavity supermodes. Apparently, at smaller gaps g, these positions depend stronger on the angular/wavelength parameter than at large g, leading to the narrower peaks.

4.4. Filter without direct coupling of the cavities

For increasing distance s the two-cavity system becomes decoupled. Here, we only refer to the case $g = 200$ nm and fix the incidence angle at $\theta = 57.56°$, i.e at the resonant angle of the single cavity. Sweeps over the cavity distances s for fixed gap and incidence angle are shown in Figure 8(a). At specific values of s the structure achieves full forward drop, while otherwise (beyond a certain distance $s \approx 500$ nm) the power is quartered. Also at the remaining outputs (not shown), with the exception of the regions around the specific s with full forward drop, the outgoing power stays roughly constant at 25% at each port. Hence, here the composite system behaves similar to the single cavity from Section 3 at resonance. Some corresponding field plots for "doubly-resonant" configurations are shown in Figure 8(b).

The "periodic" dependence $P_C(s)$ of the distance s and the corresponding power strengths can also be justified by semi-analytical arguments. For suitable large cavity distances we can divide the overall system into three subsystems: a resonator with a single cavity as introduced in Section 3 (left cavity of the complete system), a system consisting of two parallel uncoupled, "far away" straight slab waveguides and another resonator with a single cavity (right cavity of the

OSA CONTINUUM

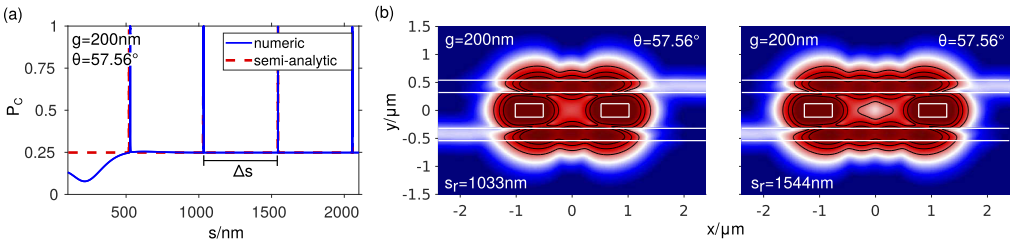

Fig. 8. Outgoing power P_C in the forward drop port over the cavity distance s for fixed gap $g = 200\,\text{nm}$ and incidence angle $\theta = 57.56°$ (a) and corresponding logarithmic field plots of the absolute electric field $\log_{10}|\boldsymbol{E}|$ at resonance (b).

complete system). In order to describe the behavior of the overall configuration with two cavities, we combine the three subsystems by semi-analytical methods. The behavior of a single cavity is described by the scattering matrix from Section 3 at resonance, calculated numerically with COMSOL. Furthermore, in the region between the cavities we can assume harmonic forward and backward propagating fields with a dependence $\sim e^{\pm ik_x x}$ on the x-coordinate with wavenumber k_x as introduced in Section 2 By combining the three elements, we can describe the behavior of the composite system. The result is shown in Figure 8(a) by the dashed line. Except for short distances s, the results fit well to the numerical COMSOL solution (solid line). For small distances the two cavities interact directly, not only through the bus waveguides. Therefore the analytical assumption of three independent subsystems is not valid and leads to different values. These semi-analytical results depend very sensitively on the calculated scattering parameters for a single cavity. Already small changes lead to considerably different values. This model now allows to predict the distance Δs of the peaks in Figure 8(a). After finding one resonating length s_r, increasing the distance between the two cavities by Δs adds another hotspot, representing the standing wave pattern, in the slab waveguide as observed in Figure 8(b) and still leads to resonance. For this reason, the periodicity of the resonance peaks is given by $\Delta s = \lambda/(2N_{TE}\cos\theta)$. For the parameters from Figure 8(a) this results in a value of $\Delta s = 512\,\text{nm}$. This value also agrees well with the numerical COMSOL calculations.

5. Concluding remarks

Theoretical approaches for the resonance behavior of a four-port rectangular microresonator have been demonstrated in a framework of a time domain coupled mode theory [10] or by general analysis of tunneling processes through localized resonant states [23,26]. It is predicted that for a specific wavelength and a configuration with one localized state (one guided mode in the cavity) half of the input power can be dropped to the upper waveguide, while the rest of the power remains in the bus waveguide or is lost to radiation. Hence this predicts an output power of 25% at each port for a lossless configuration with one cavity. Furthermore two localized states are needed, meaning an even and odd mode, to achieve full forward drop of the input power. This is forced by "accidental" degeneracy of the resonant frequencies due to the presence of the slab. Thus a lossless structure with two cavities can enable full forward drop of the incoming power.

All the results discussed in this work refer to a structure that is infinitely extended in z-direction; especially the infinite extent of the incident wave is important for the calculated results. To use this structure in real 3-D integrated photonic circuits, it is necessary to assume incoming waves confined also in the lateral direction. This is possible by considering Gaussian wave packets [12,27], or wave bundles formed by an additional rib waveguide [16], which is wide, weakly etched and placed such that it generates a semi-guided wave bundle coming in at a suitable oblique angle. These confined waves contain some range of wavenumbers in lateral direction

OSA CONTINUUM

k_z. In the limit of wide, extremely narrowband incoming beams, covering only a small range of wavenumbers, the structures act comparably to the present infinite model configuration.

Our present structures with oblique incidence angle θ realize a fully lossless setting. Accordingly, our simulations lead to results for a single cavity with quarter power in each output slab and to 100% power drop in the forward direction for the filter configuration with two cavities. In both cases fully-forward resonances are observed for specific gap distances and incidence angles, while the dimensions of the cavity are arbitrary.

Funding

Deutsche Forschungsgemeinschaft (HA 7314/1-1, TRR 142, subproject C05).

References

1. I. Chremmos, N. Uzunoglu, and O. Schwelb, eds., *Photonic Microresonator Research and Applications*, Springer Series in Optical Sciences, Vol. 156 (Springer, London, 2010).
2. B. E. Little, S. T. Chu, H. A. Haus, J. Foresi, and J.-P. Laine, "Microring resonator channel dropping filters," J. Lightwave Technol. **15**(6), 998–1005 (1997).
3. W. Bogaerts, P. De Heyn, T. Van Vaerenbergh, K. De Vos, S. Kumar Selvaraja, T. Claes, P. Dumon, P. Bienstman, D. Van Thourhout, and R. Baets, "Silicon microring resonators," Laser Photonics Rev. **6**(1), 47–73 (2012).
4. E. A. J. Marcatili, "Slab-coupled waveguides," The Bell Syst. Tech. J. **53**(4), 645–674 (1974).
5. D. R. Rowland and J. D. Love, "Evanescent wave coupling of whispering gallery modes of a dielectric cylinder," IEE Proc.-J: Optoelectron. **140**(3), 177–188 (1993).
6. M. K. Chin and S. T. Ho, "Design and modeling of waveguide-coupled single-mode microring resonators," J. Lightwave Technol. **16**(8), 1433–1446 (1998).
7. S. V. Boriskina and A. I. Nosich, "Radiation and absorption losses of the whispering-gallery-mode dielectric resonators excited by a dielectric waveguide," IEEE Trans. Microwave Theory Tech. **47**(2), 224–231 (1999).
8. M. Hammer, "Resonant coupling of dielectric optical waveguides via rectangular microcavities: The coupled guided mode perspective," Opt. Commun. **214**(1-6), 155–170 (2002).
9. M. Lohmeyer, "Mode expansion modeling of rectangular integrated optical microresonators," Opt. Quantum Electron. **34**(5-6), 541–557 (2002).
10. C. Manolatou, M. J. Khan, S. Fan, P. R. Villeneuve, H. A. Haus, and J. D. Joannopoulos, "Coupling of modes analysis of resonant channel add-drop filters," IEEE J. Quantum Electron. **35**(9), 1322–1331 (1999).
11. M. Hammer, L. Ebers, and J. Förstner, "Oblique evanescent excitation of a dielectric strip: A model resonator with an open optical cavity of unlimited Q," Opt. Express **27**(7), 9313–9320 (2019).
12. E. A. Bezus, L. L. Doskolovich, D. A. Bykov, and V. A. Soifer, "Spatial integration and differentiation of optical beams in a slab waveguide by a dielectric ridge supporting high-q resonances," Opt. Express **26**(19), 25156–25165 (2018).
13. E. A. Bezus, D. A. Bykov, and L. L. Doskolovich, "Bound states in the continuum and high-q resonances supported by a dielectric ridge on a slab waveguide," Photonics Res. **6**(11), 1084–1093 (2018).
14. M. Hammer, L. Ebers, A. Hildebrandt, A. Alhaddad, and J. Förstner, "Oblique semi-guided waves: 2-d integrated photonics with negative effective permittivity," *2018 IEEE 17th Int. Conf. on Math. Methods Electromagn. Theory (MMET)*, pp. 5–9 (2018).
15. M. Hammer, L. Ebers, and J. Förstner, "Oblique quasi-lossless excitation of a thin silicon slab waveguide: A guided-wave-variant of an anti-reflection coating," J. Opt. Soc. Am. B **36**(9), 2395–2401 (2019).
16. L. Ebers, M. Hammer, and J. Förstner, "Oblique incidence of semi-guided planar waves on slab waveguide steps: effects of rounded edges," Opt. Express **26**(14), 18621–18632 (2018).
17. M. Hammer, A. Hildebrandt, and J. Förstner, "Full resonant transmission of semi-guided planar waves through slab waveguide steps at oblique incidence," J. Lightwave Technol. **34**(3), 997–1005 (2016).
18. M. Hammer, "Oblique incidence of semi-guided waves on rectangular slab waveguide discontinuities: A vectorial QUEP solver," Opt. Commun. **338**, 447–456 (2015).
19. M. Hammer, A. Hildebrandt, and J. Förstner, "How planar optical waves can be made to climb dielectric steps," Opt. Lett. **40**(16), 3711–3714 (2015).
20. F. Çivitci, M. Hammer, and H. J. W. M. Hoekstra, "Semi-guided plane wave reflection by thin-film transitions for angled incidence," Opt. Quantum Electron. **46**(3), 477–490 (2014).
21. H. A. Haus and Y. Lai, "Theory of cascaded quarter wave shifted distributed feedback resonators," IEEE J. Quantum Electron. **28**(1), 205–213 (1992).
22. COMSOL Multiphysics GmbH, Göttingen, Germany. https://www.comsol.de.
23. S. Fan, P. R. Villeneuve, J. D. Joannopoulos, and H. A. Haus, "Channel drop tunneling through localized states," Phys. Rev. Lett. **80**(5), 960–963 (1998).
24. S. Fan, P. R. Villeneuve, J. D. Joannopoulos, and H. A. Haus, "Channel drop filters in photonic crystals," Opt. Express **3**(1), 4–11 (1998).

OSA CONTINUUM

25. M. A. Popović, C. Manolatou, and M. R. Watts, "Coupling-induced resonance frequency shifts in coupled dielectric multi-cavity filters," Opt. Express **14**(3), 1208–1222 (2006).
26. S. Fan, P. R. Villeneuve, J. D. Joannopoulos, M. J. Khan, C. Manolatou, and H. A. Haus, "Theoretical analysis of channel drop tunneling processes," Phys. Rev. B **59**(24), 15882–15892 (1999).
27. M. Hammer, A. Hildebrandt, and J. Förstner, "Full resonant transmission of semi-guided planar waves through slab waveguide steps at oblique incidence," J. Lightwave Technol. **34**(3), 997–1005 (2016).